scientific reports

Check for updates

OPEN

Integrated geophysical and geospatial techniques for surface and groundwater modeling

Ali Yousaf Khan[1], Waheed Ullah[2]✉, Abrar Niaz[1], Tehmina Bibi[1], Muhammad Mubashar Imtiaz[1], Rashida Fiaz[3], Shehla Gul[4], Kiran Hameed[5] & Fakhrul Islam[6]

An integrated approach using geophysical and geospatial techniques was employed to model the surface and subsurface water-bearing strata and assess aquifer vulnerability in the Sehnsa town, Kotli district, State of Azad Kashmir, Pakistan. The inadequate scientific studies in the hilly terrain with such complex geological conditions has led to the failure of the boreholes for groundwater extraction. For the evaluation of groundwater potential and subsurface lithology, 30 vertical electrical soundings (VES) stations utilizing the Schlumberger electrode configuration were completed, modeled and analyzed spatially. Numerous geoelectrical parameters like true resistivity, thickness of subsurface layers and Dar-Zarrouk parameters were evaluated. The subsurface lithology delineated comprised topsoil, clayey sand, sandstone, and boulder clays which closely resemble to the borehole lithologs available in the study area. The inversion model confirms the presence of patches of high-resistivity sandstone in the southwestern part of the study area with the maximum thickness of the aquifer up to 140 m. Most aquifers were classified as unconfined with Q–type resistivity curves. The protective overburden capacity of the aquifers is rated as poor at VES 1, 3–5, 8, 10–16, 18, 19, 22–25, 27 and 30 whereas the moderate category was found at VES 2, 9 and 20 and excellent at VES 7 and 28, respectively. Therefore, the VES stations with poor and moderate ratings of overburden protective capacity are vulnerable for surface contaminants. The aquifer recharge was associated with rainfall and partly from the Poonch River. The effective integration of geophysical and geospatial techniques in this study provides sufficient information about the regional water resources and gives a preliminary model that can facilitate efficient water resource management in the area. These approaches can be successfully applied to diverse geographical and hydrogeological sites due to their versatility and reliability.

Keywords Groundwater potential, Schlumberger, Geospatial, Surface water, Vulnerability, Vertical electrical sounding

Water plays a vital role in the life of every living organism[1]; with the increase in population and urbanization requirement for safe water resources is increasing; additionally, high extraction has put subsurface as well as surface water resources under immense pressure[1–4]. With increased demand, efforts have been put in to map the water distribution. Another growing problem is the deterioration of the underlying aquifer system due to excessive pumping and contaminant infiltration. It is an essential part of the groundwater surveys to delineate the surficial areas which can lead to the cause of groundwater or aquifer contamination[2,5–7]. Many conventional and non-conventional methods have been used worldwide to map water-bearing zones and for aquifer vulnerability assessment. The vertical electrical sounding (VES) method has been proven to be the best reliable solution for groundwater-related issues including exploration and vulnerability assessment[8–13]. The VES method has been widely used for groundwater extraction in fissured and permeable media channels[14,15]. The apparent resistivity field data acquired by VES generates pseudo-section plots by contouring. The pseudo section is helpful in showing the apparent resistivity values in a pictorial frame and as an underlying aide for further quantitative elucidation[16–18]. The vertical electrical sounding technique is considered to be a low-cost alternative for groundwater potential mapping in any region[19–21].

The integration of Geographic Information System (GIS) and Geoelectrical techniques have been used for the aquifers study and well site selection. Moreover, these are proven low-cost techniques for underground

[1]Institute of Geology, University of Azad Jammu and Kashmir, Muzaffarabad, Pakistan. [2]Rabdan Academy, Abu Dhabi 114646, UAE. [3]Women University of Azad Jammu and Kashmir, Bagh, Pakistan. [4]Department of Geography, University of Peshawar, Peshawar, Pakistan. [5]Technical University of Berlin, Berlin, Germany. [6]Department of Geology, Khushal Khan Khattak University, Methawalah, Pakistan. ✉email: wullah@ra.ac.ae

structural studies[22,23]. The complex data sets can be easily managed by the GIS tool[24–26], which is used for quick spatial data analysis of the different layers[27], including its application in modeling groundwater integration, presentation and numerical modeling[28,29]. The VES method delineated the zones of contamination with salinity and determined the extent of potential aquifers. The VES technique identified potential groundwater bearing zones and Dar-Zarrouk parameters of aquifer[30]. The VES method was used by several researchers to find the Dar-Zarrouk Parameters as well as hydraulic parameters of different areas[31]. The VES method was successfully used for delineation of subsurface saturated zones as well as the lithological units. The Dar-Zarrouk parameters were estimated and hydraulic parameters were calculated to find the storativity and transmissivity of subsurface materials[32–34].

The study area comprises of Sehnsa town, District Kotli which is part of Pakistani Administrated Kashmir. The current research area contains complex topography as well as geological conditions. Although, the vertical electrical sounding (VES) is applied for the demarcation of subsurface groundwater potential. This technique is also known as non-destructive technique (NDT) geophysical technique. However, there was a research gap in the study area concerned with groundwater investigation. So, the study area was not explored for groundwater through integrated geophysical and remote-sensing techniques. Therefore, keeping in the view above mentioned research gaps and local community need, the integrated geophysical and remote-sensing study was carried out.

The area's population mostly relies on groundwater extraction for domestic and agricultural use. The present study focused on integrating geophysical techniques such as VES with integrated remote-sensing techniques to identify the subsurface water-bearing zones, subsurface lithological characteristics, effects of urbanization on surface, groundwater zones and aquifer vulnerability. Geospatial techniques were utilized to generate the urbanization map and to extract watershed maps to answer any queries related to surface hydrology.

Study area

The study area is located in Sehnsa town in Kotli District, Azad Kashmir. The surveyed area is sandwiched between the 33° 27′ 50.40″ N to 33° 31′ 44.40″ N and Longitude 73° 47′ 24.00″ E to 73° 42′ 54.00″ E on Geological Survey of Pakistan toposheets no. 43G/10, 43–G/14 and 43–G/15. The study area is located in northern Pakistan including Kashmir Basin and covers nearly an area of 325.8 km^2. The area under evaluation is situated in the Sub–Himalayan region and mostly consists of molasse deposits named Siwaliks[35,36]. Dhok Pathan Formation, Nagri Formation, and the Surficial Deposits are also spread throughout the area (Fig. 1). The Nagri Formation is composed of sandstone and alternative clays. The study area is surrounded by hilly terrain and rough topography that was considered during the data acquisition. The research helped local drillers and policy-making authorities to identify safe drinking zones for the local community and to avoid the dry bore holes. The study area includes a thick sequence of sandstone exposed at Tharachi, Chamkhar, northeastern side of Sehnsa and up to some extent in the southwestern part of Sehnsa[37]. The Dhok Pathan Formation mainly comprises approximately an equivalent proportion of sandstone and shale or clays representing the typical cyclic deposition. Dhok Pathan Formation is visible in Garhuta, Galjur, Chanair and some areas of Sehnsa in the study area[35,36]. The surficial deposits include wind–blown sand, alluvial fans, rounded pebbles and gravels, recent floodplain deposits and lacustrine deposits (Table 1). There are total of 30 vertical electrical sounding (VES) stations in the study area among which 9 VES stations e.g., VES 6, 28, 16, 29, 30, 26, 12, 11 and 13 are located on the Surficial Deposits while 15 VES stations e.g., VES 23, 24, 17, 18, 20, 21, 15, 19, 3, 7, 8, 9, 10, 14 and 27 lie on Dhok Pathan Formation which contain 50% sandstone and 50% clays portions in it. Only 6 number of VES stations e.g., 1, 2, 4, 5, 22 and 25 lie on the Nagri Formation which contain 60% sandstone portion and only 40% clay portion in it.

The study area mostly contains clastic-originated sedimentary rocks e.g., gravel, clay and sand deposits. The groundwater-holding rock bodies consist of gravel, sand, sandy clay, and boulder clay. The reported rainfall per annum in the area is 1300 mm[39]. The natural phenomena of rainfall act as the main recharging source of subsurface aquifers, nalas and seasonal tributaries. In the case of our study, the Poonch River is considered an efficient recharging source for groundwater[40].

Materials and methods

Electrical resistivity data acquisition and modelling

The Fig. 2 presents the methodological approach for achieving the results of objectives in current study. The current study involves two phases e.g., Phase-I and Phase-II. The Phase-I consists of establishment of 1D electrical resistivity survey (ERS) using vertical electrical sounding (VES) technique. The acquired 1D resistivity data was the processed through computer software and then plotted in Surfer (V. 25) software for analyzing the spatial distribution of geo-electrical parameters. Similarly, the Phase-II involves the acquisition of Landsat-8 satellite imagery and SRTM-1 Arc Imagery from USGS Earth Explorer for the landcover classification and topographical and stream order analysis.

The vertical electrical sounding (VES) method was conducted in the study area at an interval of around 300 m. The subsurface resistivity (Ωm) was measured in the response of current flow by subsurface materials [42] (Fig. 3).

The apparent resistivity can be expressed in the following equation.

$$\rho a = R \times K \tag{1}$$

where

$$K = \frac{\Delta V}{I} \tag{2}$$

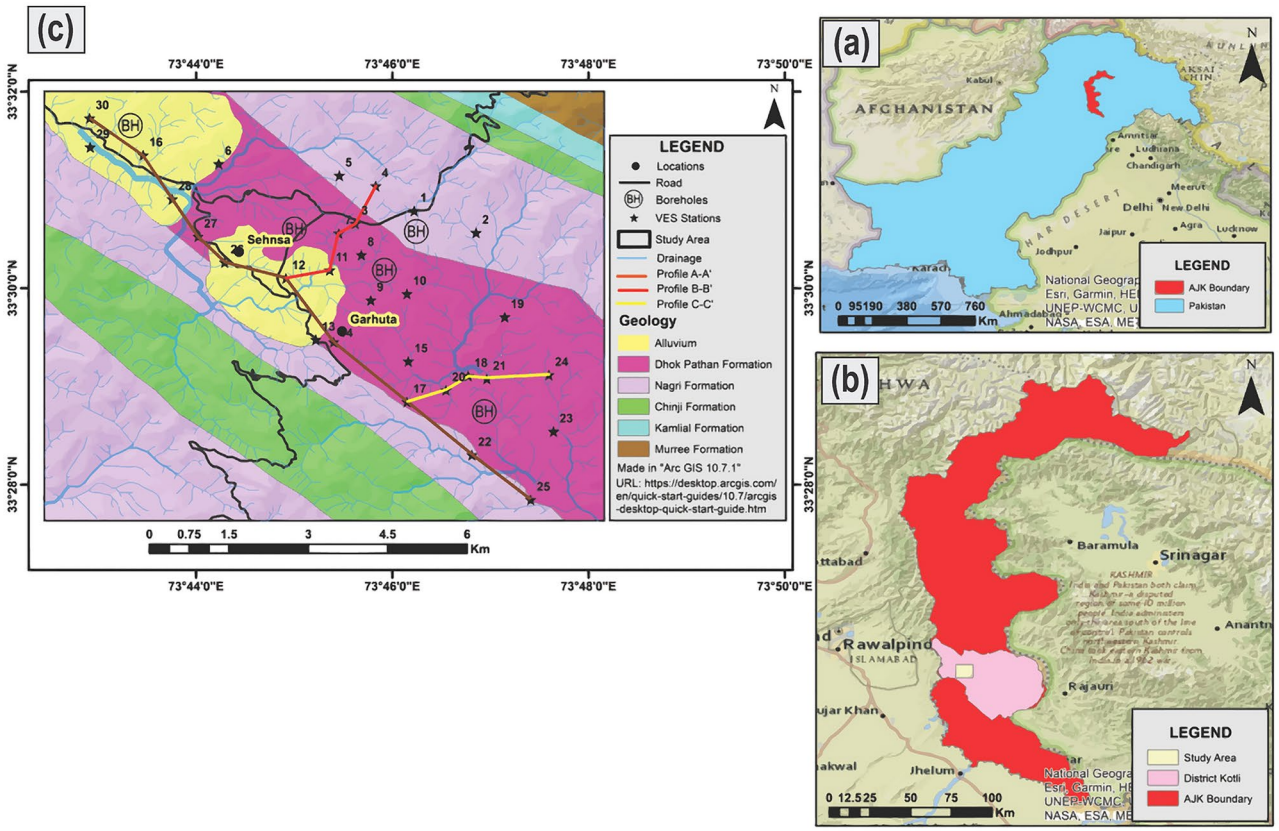

Fig. 1. (**a**) Pakistan with State of Azad Jammu and Kashmir shown by red color, (**b**) State of Azad Jammu and Kashmir with pink color showing District Kotli and yellow polygon representing study area, (**c**) Geological map of the area[38].

Formation	Age	Lithology
Surficial deposits	Recent unconformity	Unconsolidated Clay, Silt and Gravel
Dhok Pathan formation	Early pliocene to late miocene	50% sandstone and 50% Clays
Nagri formation	Late miocene	60% sandstone and 40% Clays

Table 1. Geology of the study area[41].

Combining Eqs. (1 and 2), we get

$$\rho a = R \times K \left(\frac{\Delta V}{I} \right) \tag{3}$$

V = Potential difference in milli volts. I = Applied Current in milli amperes. ρa = Apparent resistivity (ohm-meter) values. K = Geometrical Factor.

The VES method is considered to be an efficient conventional geophysical method for the delineation of groundwater potential. The current study used the ABEM SAS Terrameter 4000. A total of 30 VES stations were acquired using a Schlumberger configuration. The present study utilized the VES approach with the Schlumberger configuration to effectively differentiate between multiple geo-electrical parameters[43–46] in the identification of water bodies by using geophysical-based Rockworks software[47,48] and also hydraulic properties of aquifers. The Schlumberger configuration was chosen to find the lateral as well as vertical variations in the study area.

To analyze the resistivity data, several computer software programs were employed including IPI2WIN (2016), Exelis ENVI (5.3), Surfer (25), Arc GIS (10.7), and Rockworks (17). IPI2WIN (2016) software was specifically used for plotting and processing geo-electrical data. The different geo-electrical parameters were extracted through the true resistivity and thickness of different subsurface layers drawn by IPI2WIN (2016)

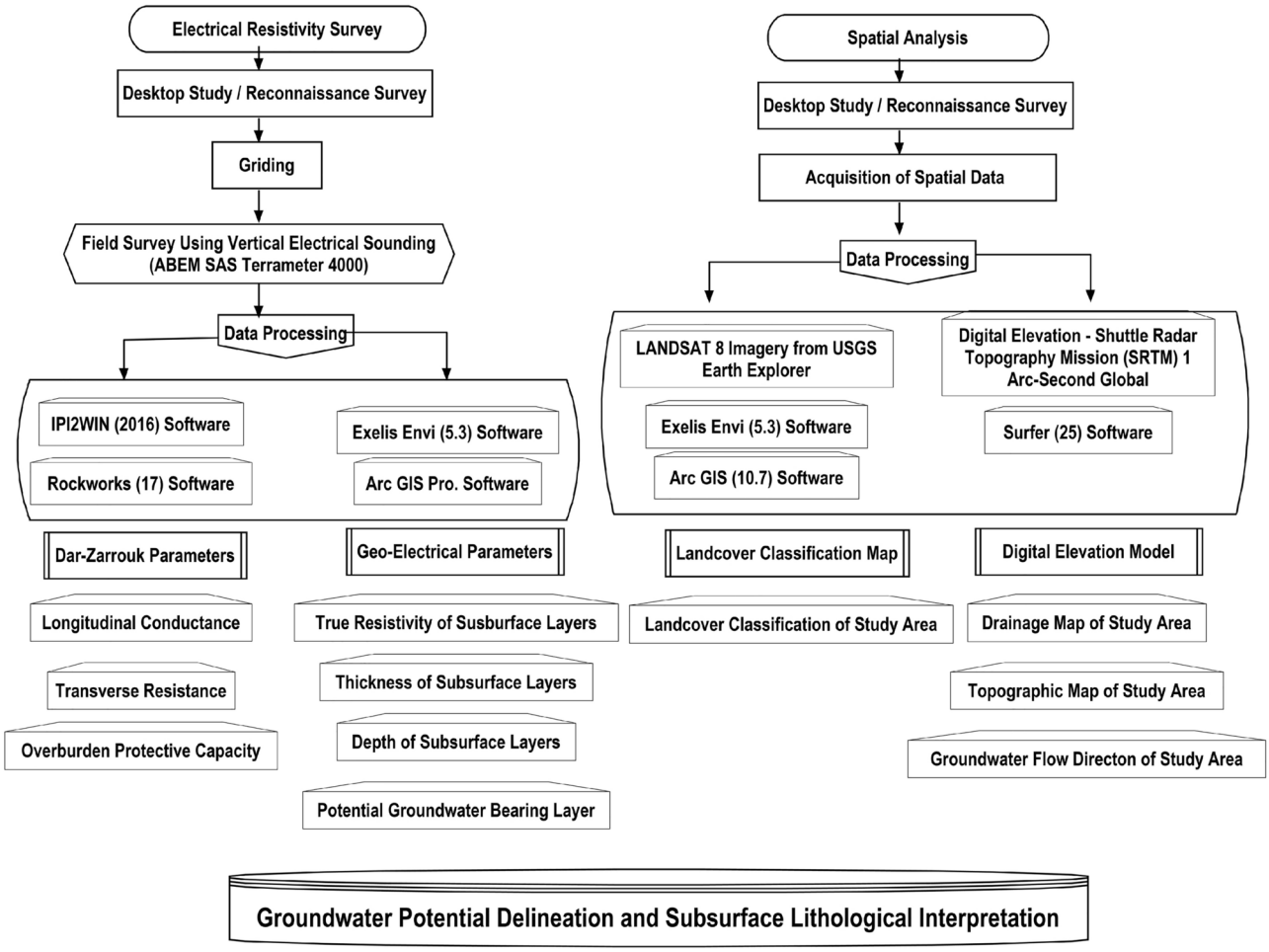

Fig. 2. Flowchart of methodology adopted for in the current study.

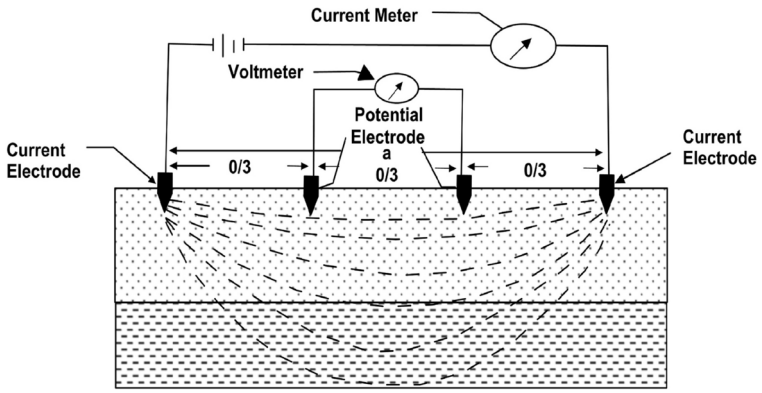

Fig. 3. Schematic diagram of vertical electrical sounding (VES) method by using Schlumberger configuration.

software[46,49]. The Dar Zarrouk parameters were evaluated to delineate the characteristics of subsurface aquifers. The partial curve matching technique was used to quantitatively interpret smooth curves taken through the set of data points. Different types of sounding curves were revealed during the processing of the resistivity data indicating the presence of variegated lithology in the subsurface. The subsurface lithological layers contain the following curve types; QQQ, $\rho1 > \rho2 > \rho3 > \rho4$; HA $\rho1 > \rho2 < \rho3 < \rho4$; HKHK $\rho1 > \rho2 < \rho3 > \rho4 < \rho5 > \rho6$ comprises of four to six layer curves; "ρ" stands for true resistivity of the layer (Fig. 4).

Spatial electrical resistivity maps were generated from the modeled one-dimensional (1D) electrical resistivity models at various depths (i.e., 2, 6, 10, 25, 40, 50, 80, 100, 150 and 200 m).

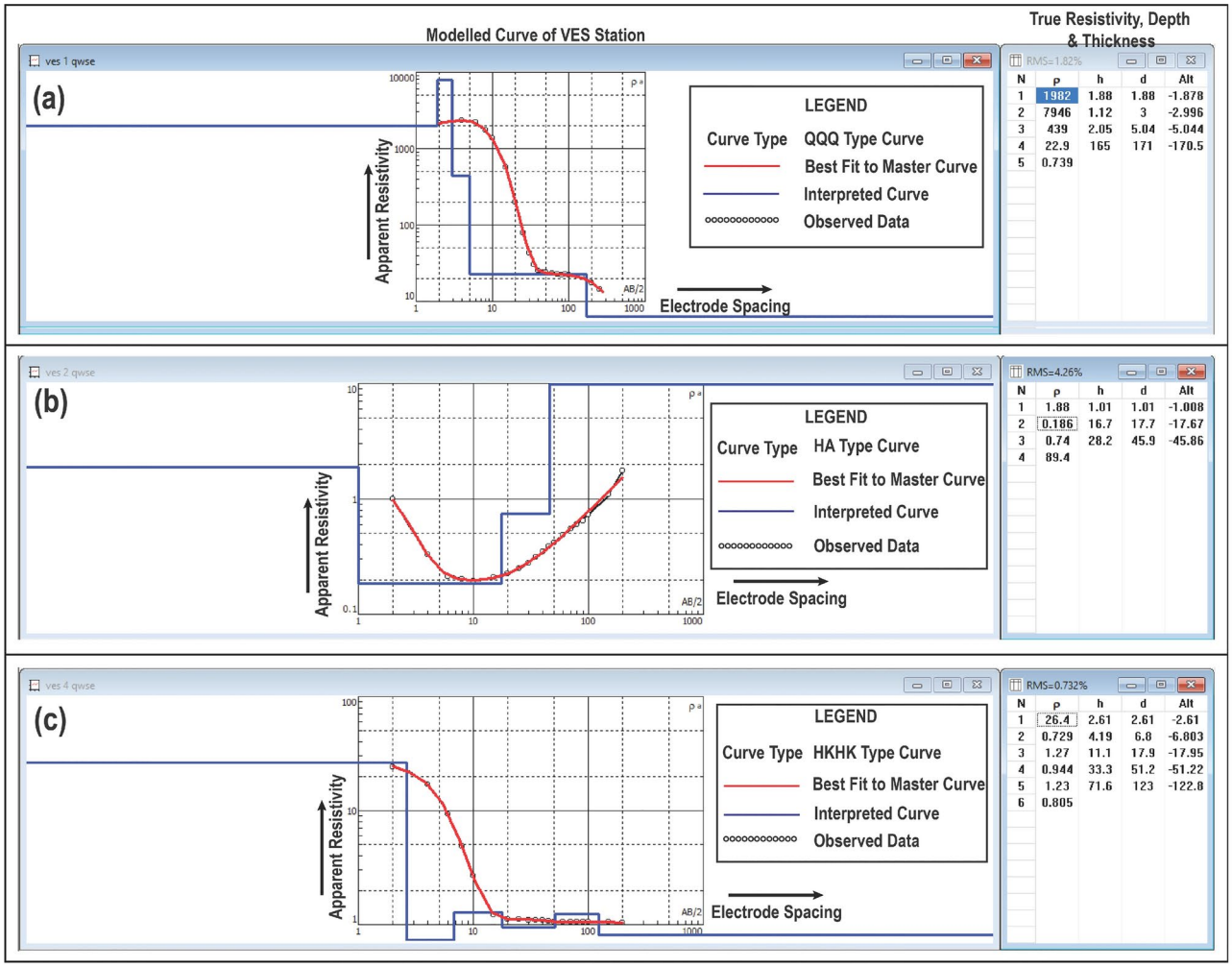

Fig. 4. The labelled diagram of typical four to six layered sounding curves of the VES 1, 2 and 3.

Dar-Zarrouk Parameters including transverse resistance and longitudinal conductance were also deduced from the 1D electrical resistivity model.

Longitudinal conductance

"Longitudinal Conductance" is considered one of the most significant geo-electrical parameters which can be stated as "the conductance in the direction of a bedding plane through a column of 1 m". The symbol "S" (Siemens) is given to this term[50,51]. The flow of the current is governed by Ohm's Law whereas Darcy's Law states about the mechanism of groundwater flow and therefore the electric and hydraulic parameters relation is generally accepted[52].

$$S = \frac{h}{\rho_a} \tag{4}$$

The total longitudinal conductance can be obtained by:

$$S_L = \sum_{(i=1}^{n} \left(\frac{h_i}{\rho_i}\right) = \frac{h_1}{\rho_1} + \frac{h_2}{\rho_2} + \frac{h_3}{\rho_3} + \ldots + \frac{h_n}{\rho_n} \tag{5}$$

where "h" stands for the thickness of each layer and "ρ" stands for the resistivity of each layer.

Transverse resistance

The transverse resistance of the resistive layer and conductance of the conducting layers are determined in terms of transverse resistance and longitudinal conductance, respectively[46]. It is symbolized by capital alphabetical

Type	Date	Latitude	Longitude	Cloud cover	Satellite row	Satellite path
Landsat 8 imagery	15th Sept. 2016	33.17677° N	74.43642° E	3.14%	37	149

Table 2. Detailed description of Landsat 8 imagery used for extraction. Obtained from USGS earth explorer

letter "T" (in Ωm^{-1}) and can be explained as the resistance over a l m column which is perpendicular to the plane[50].

$$T = h.\rho_a \tag{6}$$

The total transverse resistance formula can be obtained by:

$$T_L = \sum_{i=1}^{n} h_i.\rho_i = h_1.\rho_1 + h_2.\rho_2 + h_3.\rho_3 + \ldots + h_n.\rho_n \tag{7}$$

Since "ρ" and "h" stands for true-resistivities and thickness correspondingly whereas "N" denotes number of sub-surface geological layers. "T" stands for transmissivity therefore the higher values of "T" generally reflect high aquifer transmissivity.

Geospatial data acquisition and processing

The Landsat 8 imagery was acquired from USGS earth explorer website (U.S. Geological Survey. (2023, September 4). Earth Explorer. Retrieved from https://earthexplorer.usgs.gov/). The geospatial based software "Exelis ENVI (5.3)" and Arc-GIS (10.7) were employed for generation of land cover map. Topographic maps as well as drainage maps of the study area have been generated through Arc-GIS (10.7) through Digital Elevation Model (DEM). Various corrections including radiometric and geometric corrections were made on LANDSAT-8 imagery. Moreover, the calibration and DOS tools were also used to enhance these imageries. The final land cover map was generated with 5 classes (Fig. 9). The water recharging bodies can be observed in the resulting map (Fig. 8). The detailed description of landcover map is given below in Table 2.

The Surfer (25) contouring software was used to generate the iso–resistivity maps at various depths. Three-dimensional sub-surface models and fence diagrams of the area were generated through Rockworks (17) software. Similarly, the resistivity inversion model was produced by using Arc GIS Pro which enabled us to view the subsurface block diagram in three-dimensional view.

Landcover map

The landcover map will be prepared by using the Landsat 8 imagery which was obtained by USGS Earth Explorer website. The properties of Landsat 8 imagery are given in Table 2.

Topographic and drainage map

The topographic map is prepared by using the DEM having pixel size of 30 m in Arc-GIS (10.7) software. The DEM was acquired from https://earthexplorer.usgs.gov/. The elevation have the vital role in the deposition of the sediments under the action of gravity[45].

Results

The study area exhibited typical three to six layered VES curves. At each VES point, the lithological column was estimated, considering factors such as layer thickness, resistivity, and depth. The identified geological layers consisted of gravel, sand, topsoil (sandstone), and clay (Table 3). The second and third layers predominantly consisted of high-resistivity sandstone, ranging from 208 to 6560 Ωm, indicating the presence of compacted sandstone in the area[50,53]. The aquifer thickness map (Fig. 6d) shows that the values are elevated in northeastern portions of current area that verifies sufficient groundwater potential. The geological data lies closely to the computed geological model[50]. The qualitative and quantitatively interpretation of resistivity data has been carried out.

Borehole lithologs

There were limited borehole lithologs (Fig. 1) available in the study area. However, five lithologs were acquired in the study from different locations e.g., BH-01, BH-02, BH-03, BH-04 and BH-05, respectively. The borehole BH-01 was located near the Government Girls Primary School Sehnsa and situated on the Nagri Formation which contain the mix proportion of sandstone (60%) and clay (40%). The borehole BH-02 was located near Main Bazar British Council Language School. The borehole BH-03 was located near Kotla at Chichlar Road. The borehole BH-04 was located near Garotha. The boreholes BH-02, BH-03 and BH-05 were situated on the Dhok Pathan Formation with mix proportion of sandstone (50%) and clay (50%). Similarly, the borehole-05 was located near Bhrand. This borehole was situated on the Surficial Deposits or Alluvium which contain unconsolidated deposits of clay, silt, sand and gravels. The gravels of the Surficial Deposits in BH-05 are acting as an aquifer while the conglomerate and sandstone (weathered) in the boreholes BH-01, BH-02, BH-03 and BH-04 are acting as the aquifer. The lithologs of all boreholes are presented in the Fig. 5.

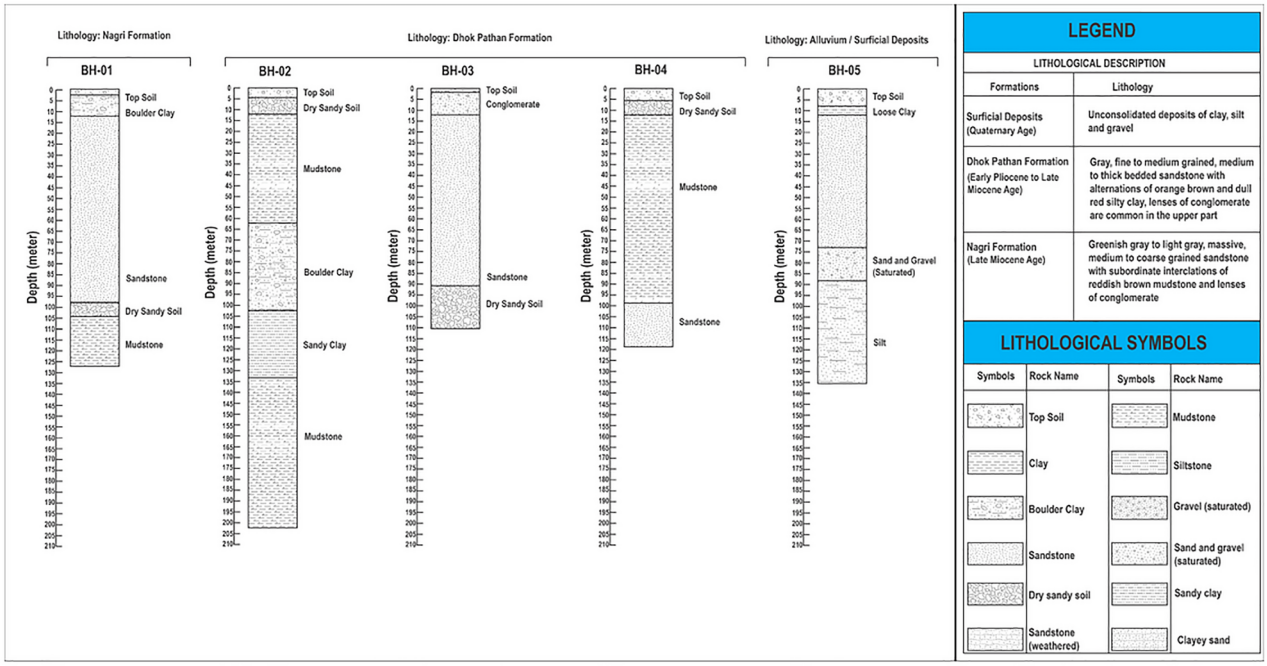

Fig. 5. Lithologs of boreholes obtained from the study area.

Electrical resistivity models

Iso-resistivity model

The extent and presence of groundwater can be calculated by an important factor of apparent resistivity. According to the Pal and Majumdar, it is quite promising to delineate the areas with various groundwater quality by mapping of iso–resistivity data[54]. The maps of apparent resistivity at 2, 6, 10, 25, 40, 50, 80, 100 and 150 m with resistivity ranges from 1.0002 to 991.29 Ωm were generated. A comparison of these maps is shown in the Fig. 6. The high values of apparent resistivity are found in central and southern portions. The northern part of study area delineated low apparent resistivity and hence delineating good potential of fresh water in this part (comparatively loose material consisting of gravels, boulder clays and sand). These maps also portrayed that the groundwater potential increases with depth. The iso-resistivity maps ranging in depth from 25 m to the depth of 140 m show good groundwater potential at central portion due to the presence of low-resistivity closures.

2D electrical resistivity cross section

The lithological cross sections are drawn in the Fig. 7. The Fig. 6 represents the lithological cross sections of Profile A-A′, B-B′ and C-C′. The Profile line A-A′ is in the northwest to southeast direction and comprised of VES 30, 16, 28, 27, 26, 12, 14, 27, 22 and 25 while the Profile line B-B′ is in the northeast to southwest direction and comprised of VES 4, 3, 7, 11 and 12. Similarly, the Profile line C-C′ is also in the northeast to southwest direction and comprised of VES 24, 21, 1 20 and 17. The total length of Profile A-A′ is 10 km, Profile B-B′ is 2.5 km and that of Profile C-C′ is 2 km respectively. The Profile line A-A′ has high resistivity values which are associated with sandstone, mudstone at VES 30, 22 and 25 respectively. Similarly, the Profile line B-B′ has high resistivity rocks e.g., sandstone at VES 3 up to the depth of 20 m. The VES 11 of Profile line B-B′ has intermediate rocks e.g., mudstone up to the depth of 140 m. The Profile line B-B′ has lowest values of apparent resistivity at VES 7 which are associated with water saturated rocks. The Profile Line C-C′ has high resistivity values at VES 24 up to the depth of 20 m and at VES 1 with depth of 40 m. These high resistivity values of rocks are associated with the presence of compact sandstone.

3D electrical resistivity inversion model

Figure 8 represents apparent resistivity inversion model of the study area which was prepared in Arc GIS Pro software. The total depth of this model is 200 m, respectively. This model delineated that there is the presence of loose to intermediate strata on the top layer of study area on the northeastern portion of study area. The area has low resistivity material on northeastern portion while intermediate to hard material is present on southwestern portion. The inversion model confirms the presence of patches of high resistivity sandstone in the southwestern side of study area. While the consecutive beds of sandstone and clays are shown in the southern portion of study area.

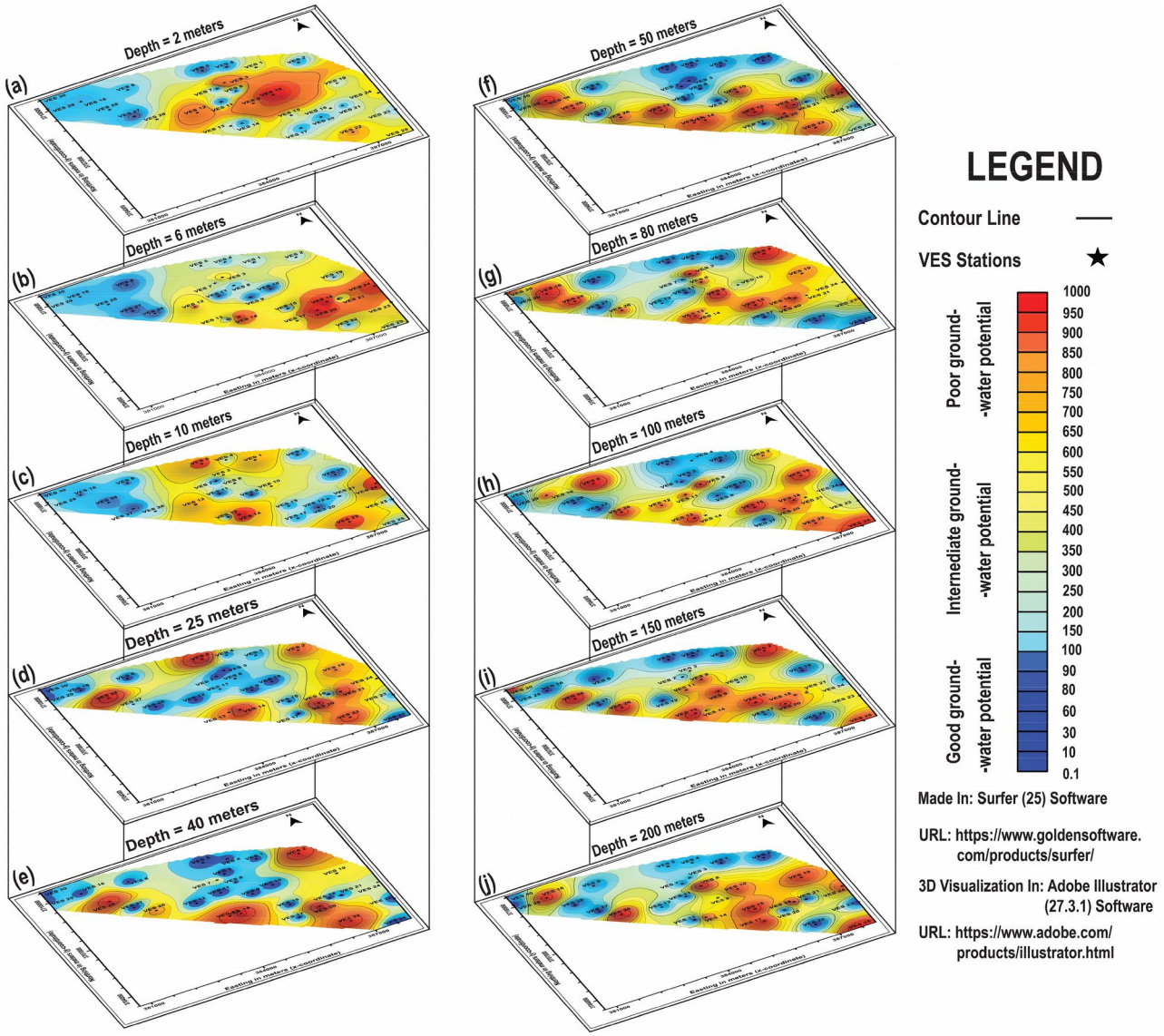

Fig. 6. Comparison of iso–resistivity maps at numerous spacings of electrodes. (**a**) 2 m, (**b**) 6 m, (**c**) 10 m, (**d**) 25 m, (**e**) 40 m, (**f**) 50 m, (**g**) 80 m, (**h**) 100 m, (**i**) 150 m, (**j**) 200 m.

Dar Zarrouk parameters

Longitudinal conductance

The high values of longitudinal conductance commonly represent the thick succession and therefore, special care should be given the highest priority in the evaluation of groundwater potential. The total longitudinal conductance parameter is represented in the Fig. 9a. The values range among 0 to 7050 mhos. The value of conductance rises towards north–eastern part of study area indicating the presence of unconsolidated material of Nagri Formation. However, the decrease in resistivity as well as the increase in conductance typically represents the potential groundwater aquifers[55,56]. The Dar-Zarrouk Parameters of the study area are shown in the Table 5.

There is a direct relation between the overburden protective capability of an aquifer and its hydraulic conductivity[45]. The clayey material which blocks movement of fluid is typically represented by the low hydraulic conductivities as well as low resistivities and low values of unit longitudinal conductance[44,53]. Table 3 presents the protective capacity ratings. The clay overburden ratings are presented in Table 4

Figure 9b represents "unit longitudinal conductance" map of study area. According to Fig. 5 which represents the aquifer vulnerability the protective capacity ratings at VES stations 1, 3, 4, 5, 8, 10, 11, 12, 14, 15, 17, 18, 21, 22, 23, 24, 26 and 30 are poor, indicating that these segments are classified by thin layers or no shale. Therefore, aquifers at these locations are vulnerable to leaching toxic fluids from surface[61,62]. Likewise, protective capacity at VES 9 and 13 is ranked as weak, while at 6, 16 and 28 are ranked as moderate, at 19, 25 and 29 is ranked as good and excellent at 2, 7, 20 and 27 respectively. Therefore, it shows the low vulnerability risk at those sites. It

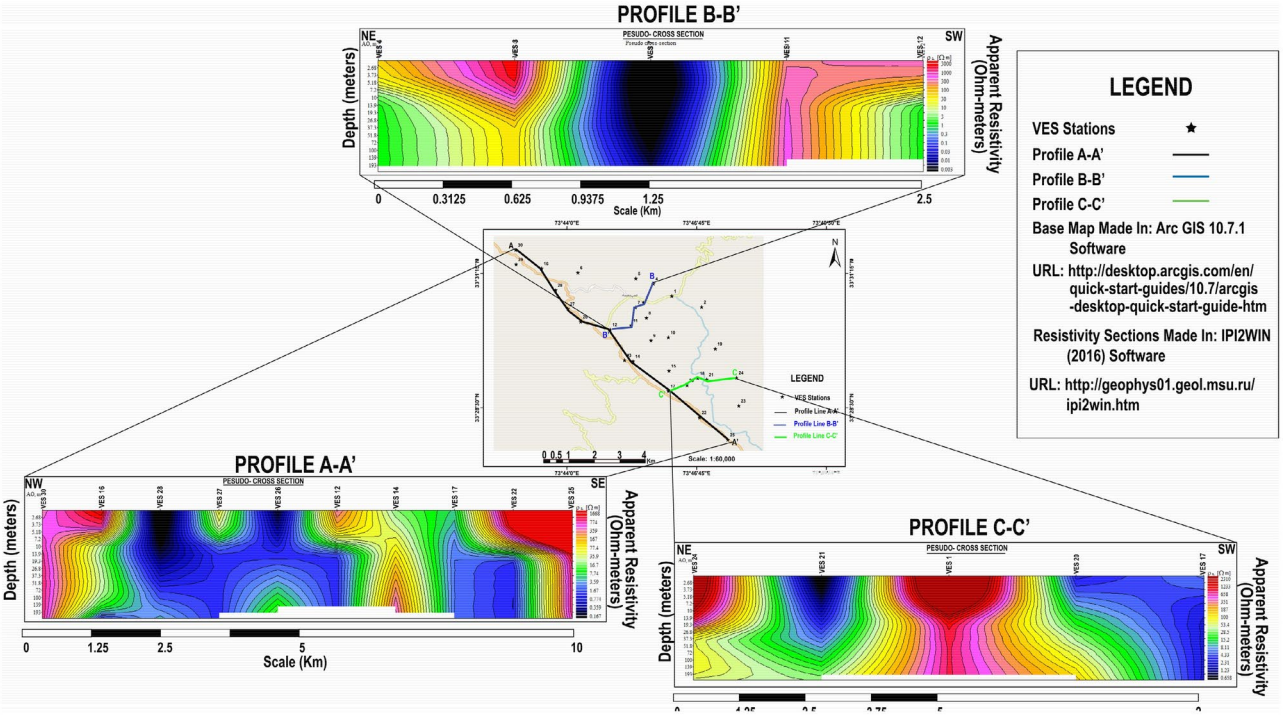

Fig. 7. Lithological cross sections of Profile A-A′, B-B′ and C-C′ along with base map of study area.

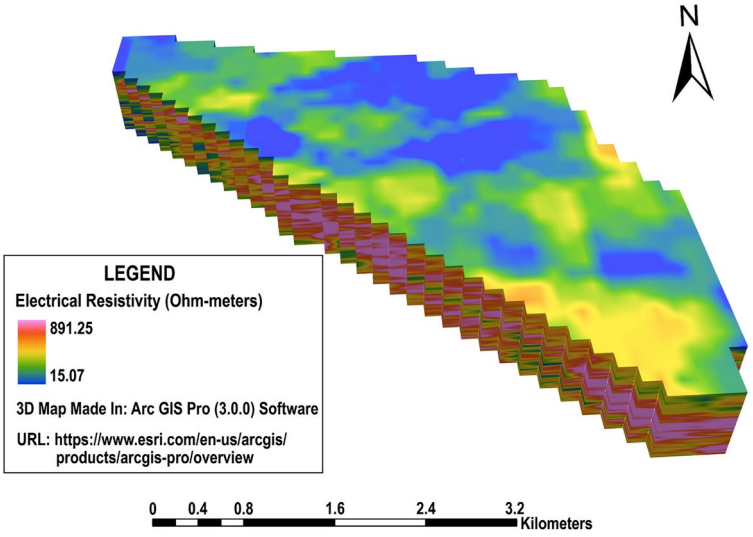

Fig. 8. Apparent resistivity inversion model.

VES no	Coordinates		Root mean square error	Geological formation	Curve type	Layers No	Resistivity (Ωm)	Lithological interpretation	Thickness (m)	Depth (m)
	Latitude (N)	Longitude (E)								
1	33.513111°	73.770389°	1.82%	Nagri Formation	KQQ	1	1982	Top Soil	1.88	1.88
						2	7946	Sandstone	1.12	3
						3	439	Mudstone	2.05	5.04
						4	22.9	Boulder Clay	165	171
						5	0.74	Clay	–	–
2	33.509389°	73.780917°	4.26%	Nagri Formation	HA	1	1.88	Top Soil	1.01	1.01
						2	0.186	Clay	16.7	17.7
						3	0.7	Clay	28.2	45.9
						4	89.4	Mudstone	–	–
3	33.510944°	73.760389°	0.935%	Dhok Pathan Formation	KQ	1	2726	Sandstone	1	1
						2	4034	Conglomerate	1.64	2.64
						3	325	Mudstone	6.2	8.84
						4	41.5	Boulder Clay	–	–
4	33.517325°	73.763859°	0.732%	Nagri Formation	HKHK	1	26.4	Top Soil	2.61	2.61
						2	0.729	Clay	4.19	6.8
						3	1.27	Clay	11.1	17.9
						4	0.944	Clay	33.3	51.2
						5	1.23	Clay	71.6	123
						6	0.805	Clay	–	–
5	33.519111°	73.757667°	1.37%	Nagri Formation	KHA	1	182	Top Soil	1	1.01
						2	710	Sandstone	2.18	3.18
						3	3.32	Clay	7.1	10.3
						4	7.06	Boulder Clay	21.8	32.1
						5	7.82	Clay	–	–
6	33.521083°	73.737194°	1.25%	Surficial Deposits	AKH	1	0.163	Top Soil	1.42	1.42
						2	0.165	Clay	1	2.54
						3	2.37	Silt	4	6.22
						4	0.521	Clay	2.95	9.17
						5	1.04	Boulder Clay	–	–
7	33.509278°	73.757583°	0.933%	Dhok Pathan Formation	HKH	1	0.0034	Top Soil	1.03	1.03
						2	0.0012	Clay	7.42	8.45
						3	0.0028	Clay	10.70	19.1
						4	0.001	Clay	30.90	50.1
						5	0.134	Clay	–	–
8	33.505639°	73.761417°	0.657%	Dhok Pathan Formation	AKHKH	1	60.2	Top Soil	1	1
						2	124	Sandy Clay	1.79	2.79
						3	834	Dry Sandy Soil	5.01	7.8
						4	399	Mudstone	14.0	21.8
						5	781	Dry Sandy Soil	39.1	60.9
						6	398	Mudstone	109	170
						7	1293	Sandstone	–	–
9	33.497944°	73.763028°	0.872%	Dhok Pathan Formation	KHK	1	3.69	Top Soil	1.00	1
						2	5.56	Boulder Clay	0.78	1.78
						3	1.33	Clay	2.9	4.7
						4	1.38	Clay	165	170
						5	1.26	Clay	–	–
10	33.499028°	73.769167°	1.73%	Dhok Pathan Formation	AK	1	118	Top Soil	2	2
						2	466	Dry Sandy Soil	86.4	88.4
						3	656	Sandstone	137	225
						4	55.2	Boulder Clay	–	–
11	33.503056°	73.756028°	0.866%	Surficial Deposits	KH	1	261	Top Soil	2.4	2.4
						2	872	Conglomerate	2.92	5.32
						3	544	Sand and Gravel	6.24	11.6
						4	654	Gravel Dry	–	–

Continued

VES no	Coordinates		Root mean square error	Geological formation	Curve type	Layers No	Resistivity (Ωm)	Lithological interpretation	Thickness (m)	Depth (m)
	Latitude (N)	Longitude (E)								
12	33.501694°	73.748611°	1.64%	Surficial Deposits	HA	1	174	Top Soil	2.5	2.5
						2	0.706	Clay	1.34	3.83
						3	1.52	Silt	124	128
						4	5.52	Boulder Clay	–	–
13	33.49125°	73.753667°	0.755%	Surficial Deposits	QHK	1	18	Top Soil	1.33	1.33
						2	10	Boulder Clay	1.17	2.5
						3	1	Silt	0.75	3.25
						4	1.12	Sand	57.6	60.9
						5	1.11	Clay	–	–
14	33.490861°	73.756694°	0.891%	Dhok Pathan Formation	AKH	1	11.7	Top Soil	1	1
						2	31	Boulder Clay	1.67	2.67
						3	643	Dry Sandy Soil	4.5	7.14
						4	569	Sandstone (weathered)	11.9	19.1
						5	643	Sandstone	–	–
15	33.487583°	73.769389°	0.92%	Dhok Pathan Formation	AAK	1	47.2	Top Soil	1	1
						2	145	Siltstone	1.790	2.79
						3	571	Dry Sandy Soil	58.1	60.9
						4	592	Sandstone	109.0	170
						5	513	Sandstone (weathered)	–	–
16	33.522556°	73.724361°	3.68%	Surficial Deposits	HKQ	1	3346	Gravel (dry)	1.54	1.54
						2	15.1	Boulder Clay	13.1	14.6
						3	72	Gravel	17.9	32.5
						4	9.46	Sand	20.6	53.2
						5	0.031	Clay	–	–
17	33.480694°	73.769167°	1.12%	Dhok Pathan Formation	QHK	1	6.93	Top Soil	1	1
						2	4.24	Boulder Clay	1.79	2.79
						3	1.93	Clay	5.01	7.8
						4	2.16	Sand	162	170
						5	1.91	Clay	–	–
18	33.485111°	73.779556°	1.45%	Dhok Pathan Formation	QQQ	1	77,978	Sandstone	1	1
						2	44,497	Sandstone	1.7	2.7
						3	2509	Consolidated Shale	4.05	6.76
						4	861	Dry Sandy Soil	129	136
						5	825	Sandstone (weathered)	–	–
19	33.495111°	73.785764°	2.1%	Dhok Pathan Formation	QHK	1	570	Sandstone	2.77	2.77
						2	44	Mudstone	3.42	6.19
						3	3.44	Clay	2.42	8.61
						4	9.89	Boulder Clay	41.1	49.7
						5	9.34	Clay	–	–
20	33.482694°	73.775778°	1.48%	Dhok Pathan Formation	AKH	1	2	Top Soil	1	1.06
						2	3	Clay	1.35	2.4
						3	697	Sandstone	6.82	9.22
						4	62	Mudstone	20.8	30
						5	406	Dry Sandy Soil	–	–
21	33.484611°	73.782722°	2.46%	Dhok Pathan Formation	AAA	1	0.935	Top Soil	1	1
						2	1.43	Sand	4.25	5.25
						3	1.46	Clay	0.4	5.65
						4	9.5	Boulder Clay	23.6	29.3
						5	67.9	Sandstone	–	–
22	33.471694°	73.780194°	2.35%	Nagri Formation	KQH	1	487	Sandstone	1	1
						2	761	Conglomerate	1.46	2.46
						3	1.08	Sand	19.3	21.8
						4	0.964	Clay	220	241
						5	1.98	Sand	–	–

Continued

VES no	Coordinates		Root mean square error	Geological formation	Curve type	Layers No	Resistivity (Ωm)	Lithological interpretation	Thickness (m)	Depth (m)
	Latitude (N)	Longitude (E)								
23	33.475694°	73.794056°	0.88%	Dhok Pathan Formation	HK	1	95.9	Top Soil	2.13	2.13
						2	6.47	Clay	0.279	2.41
						3	12.6	Boulder Clay	58.5	60.9
						4	12.1	Clay	–	–
24	33.485278°	73.793278°	0.598%	Dhok Pathan Formation	QHK	1	7470	Sandstone	2.5	2.5
						2	2160	Consolidated Shale	5.57	8.07
						3	42	Boulder Clay	19.6	27.7
						4	130	Mudstone	84.9	113
						5	0.923	Clay	–	–
25	33.464083°	73.790194°	3.67%	Nagri Formation	QQ	1	331,618	Sandstone	2	2.08
						2	2439	Consolidated Shale	3.41	5.49
						3	939	Dry Sandy Soil	221	227
						4	31	Boulder Clay	–	–
26	33.504361°	73.738194°	1.28%	Surficial Deposits	AAA	1	0.533	Top Soil	1	1
						2	0.831	Clay	1.24	3.24
						3	2.51	Sand	13.50	16.8
						4	9.7	Boulder Clay	36.3	53
						5	1151	Conglomerate	–	–
27	33.50875°	73.733667°	1.77%	Dhok Pathan Formation	HK	1	63.3	Top Soil	2.09	2.09
						2	0.422	Clay	0.83	2.92
						3	1.13	Sandy Clay	151	154
						4	0.984	Clay	–	–
28	33.515111°	73.729306°	0.845%	Surficial Deposits	KHA	1	0.16	Top Soil	2.82	2.82
						2	1.24	Sand	6.5	9.32
						3	0.953	Clay	12.3	21.6
						4	3.5	Sandy Clay	36.7	58.4
						5	36.5	Boulder Clay	–	–
29	33.523917°	73.715361°	0.813%	Surficial Deposits	AKH	1	1.19	Top Soil	2	2.06
						2	3.11	Clay	23	25.1
						3	4.07	Sandy Clay	24.1	49.2
						4	1.86	Clay	88.3	138
						5	14.7	Boulder Clay	–	–
30	33.528833°	73.71525°	1.24%	Surficial Deposits	AKH	1	341	Top Soil	1	1
						2	528	Loose sand	1.74	2.74
						3	998	Conglomerate	21.7	24.5
						4	923	Gravel (dry)	44.2	68.7
						5	949	Conglomerate	–	–

Table 3. Vertical lithological column of the study area along with different geoelectrical parameters.

has been demonstrated the fact that; minimum 10 m thicked layer of any rock e.g., shale is essential for virtuous protective capacity[49].

Transverse resistance

The transverse resistance map of the study area shows that the southeastern part of study area has the highest ranges of transverse resistance values which leads to the low groundwater potential zone (Fig. 9c). The resistivity and conductivity are generally inversely proportional to each other[57].

Aquifer thickness map

The aquifer thickness map represents the thickness of aquifer in our area. Excellent groundwater potential appears in northeastern portion. While the other portions are designated as moderate groundwater potential zones Fig. 9d. This map can be utilized in marking geological rock formations as the volume of water is dependent upon the aquifer thickness. Different colors on the legend are showing the lowest and highest values of aquifer thickness with red color indicating the high good groundwater potential while blue color representing the low groundwater potential. The area is categorized in good and fair groundwater potential zones[58].

Longitudinal conductance (mhos)	Protective capacity rating
> 10	Excellent
5–10	Very Good
0.7–4.9	Good
0.2–0.69	Moderate
0.1–0.19	Weak
< 0.1	Poor

Table 4. Modified longitudinal conductance/protective capacity rating[53].

		Geo-electrical parameters				
		Dar-Zarrouk parameters				
	Total Thickness (m)	Transverse resistance (Ωm^2)	Longitudinal conductance (Mhos/Siemens)	Transversal resistivity	Longitudinal resistivity	Anisotropy co-efficient
VES no	$H = \sum Hi$	$Ti = Hi \times \rho i$ $T = \sum Ti$	$Si = \frac{Hi}{\rho i}$ $S = \sum Si$	$Pt = \frac{T}{H}$	$PI = \frac{H}{S}$	$\lambda = \sqrt{\frac{Pt}{PI}}$
1	170.05	17,304.13	7.21	101.76	23.58	2.1576
2	45.91	58.873	161.4303	1.282357	0.284395	2.254533
3	8.84	11,356.76	0.01985	1284.701	445.3332	1.442405
4	122.80	205.5587	108.0734	1.673931	1.136265	0.736594
5	32.08	1909.067	5.231981	59.50956	6.131521	4.852757
6	9.17	10.67481	22.71447	1.164101	0.403707	1.441763
7	50.05	0.073266	41,207.7	0.001464	0.001215	0.602619
8	169.90	83,965.6	0.072142	494.206	2355.088	0.104923
9	169.70	239.6048	122.1718	1.41194	1.389019	0.508251
10	225.40	130,370.4	0.411198	578.3957	548.154	0.527585
11	11.56	6567.2	0.024015	568.0969	481.3735	0.590079
12	127.84	624.426	83.49133	4.884434	1.531177	1.594993
13	60.851	100.2588	52.50856	1.647611	1.158878	0.710865
14	19.03	9702.517	0.167018	509.8538	113.9398	2.237381
15	169.89	98,009.85	0.319404	576.9018	531.8966	0.542306
16	53.14	6839.696	3.293179	128.7109	16.13638	3.98822
17	169.8	374.1089	78.16232	2.203233	2.172402	0.507096
18	135.75	274,853.4	0.151491	2024.702	896.0928	1.129739
19	49.71	2144.184	4.941788	43.13385	10.05911	2.144019
20	30.03	6049.27	1.329814	201.4409	22.5821	4.460188
21	29.246	231.7907	6.79699	7.925551	4.302787	0.920979
22	241.76	1830.984	246.0901	7.573561	0.982404	3.854604
23	60.909	943.1721	4.70819	15.48494	12.93682	0.598483
24	112.57	42,556.6	1.128279	378.0457	99.77138	1.89456
25	226.49	905,601.4	0.236761	3998.417	956.6181	2.089871
26	52.04	387.5584	12.4891	7.447318	4.166832	0.893643
27	153.921	303.2777	135.6305	1.970346	1.134855	0.868105
28	58.32	148.6831	46.25926	2.549436	1.260721	1.011103
29	137.46	336.3064	62.52109	2.446576	2.198618	0.55639
30	68.64	63,712.92	0.075859	928.2185	904.8388	0.512919

Table 5. Dar-Zarrouk Parameters of current research work.

Lithological models of the study area

Three to four to six layered model was revealed based on subsurface resistivity data. Those layers are clay, boulder clay, clay (very dry), sand and gravel, dry sandy soil, sandstone and sandy clay[47]. Confined and unconfined nature of aquifers are delineated in current area, however most of aquifers are unconfined. The Rockworks generated lithological simulation model of our area is shown in Fig. 10a, b. Likewise, the lithology fence diagram shows the 3D pictorial view of subsurface geology as represented in the Fig. 10b.

This model encompasses the sandstone layer in southwest segment of study area as well as northeast part (Fig. 10). Unconfined aquifers (VES 1, 3–5, 8–12, 15, 17–26, 30) with top layer sand and gravel are identified

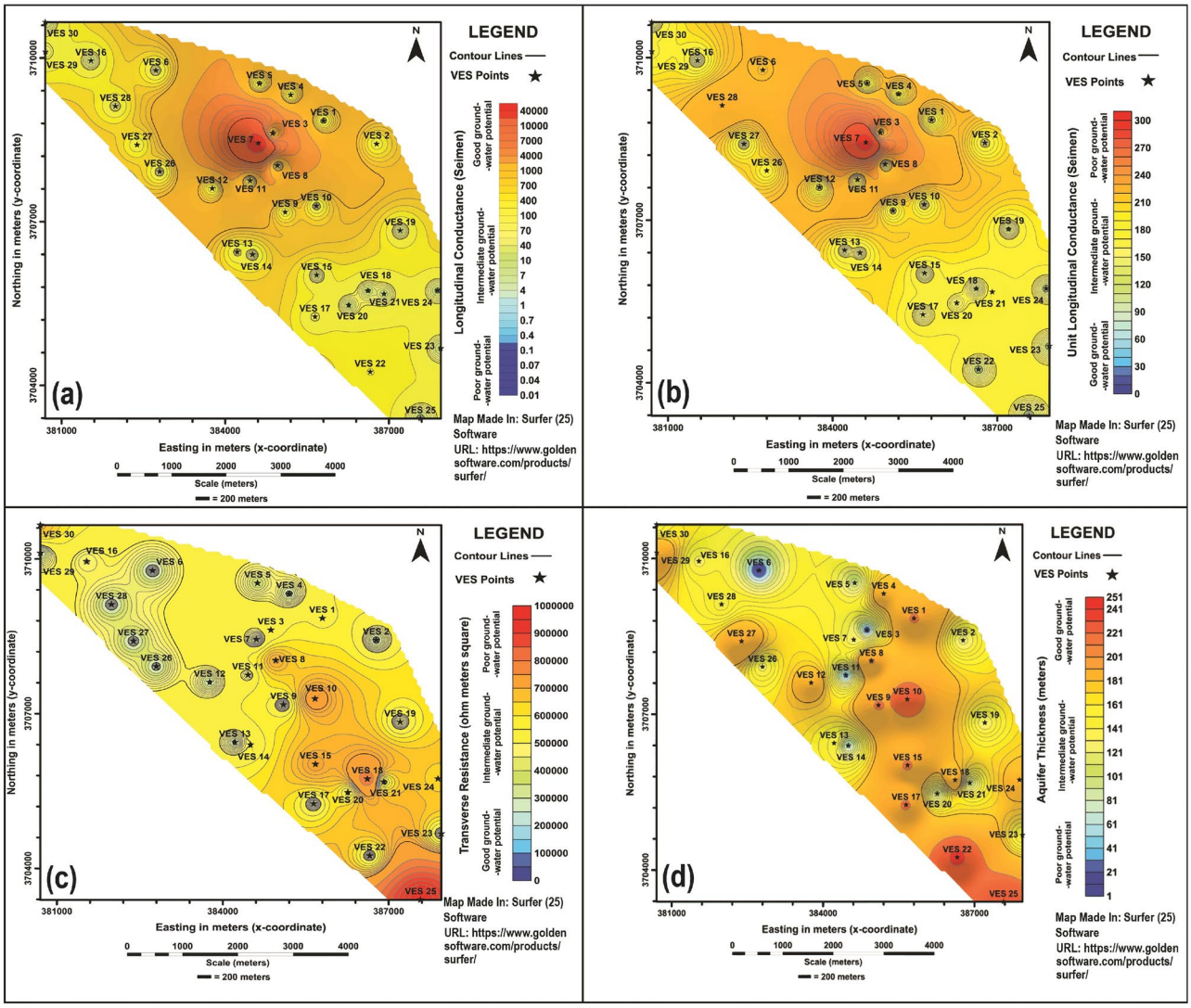

Fig. 9. (**a**) Total longitudinal conductance map, (**b**) unit longitudinal conductance map, (**c**) transverse resistance map, (**d**) aquifer thickness map.

in the southern part of the study area. Sand and gravel (brown) act as water-bearing rock bodies, boulder clay (green) and sandy clay (blue). Compact sandstone (shown in red color) is also found in northern part with low probability of groundwater with resistivity ranges from 1000 Ωm to onwards in study area (Fig. 8). The known surface geology as well as the hydrological parameters which are computed by GIS lies very closely to the generated 3D geological model by Rockworks software. The resistivity values with lower ranges are associated with the recharging agents of surface running bodies[45].

Geospatial analysis

Landcover map

The land distribution map categorizes the total area (325.8063 km^2) into five categories in terms of land distribution. Most of the area in surrounding has been covered with forests followed by grass land and urban land. The large area covered with forests and grass land serves as good recharge zones for the groundwater aquifer system, but this area mostly lies towards northeast and southwest as shown by Fig. 11. Most of the study area lies in urban land. The population in urban land not only drains large quantities of the water from aquifers but also introduces surface contamination in the groundwater system. There is the distribution of dense "Forest" and "Grass Land" classes in north-eastern and south-western side of study area which ultimately promotes the infiltration of surface or meteoric water that recharge the groundwater. These results are also indicated by the VES data sets.

Topographic and drainage maps

The topography and the drainage of the study area are presented in the Fig. 12. The study area has minimum and maximum elevation of 498 and 1130 m, respectively. The elevation varies considerably in northeast and

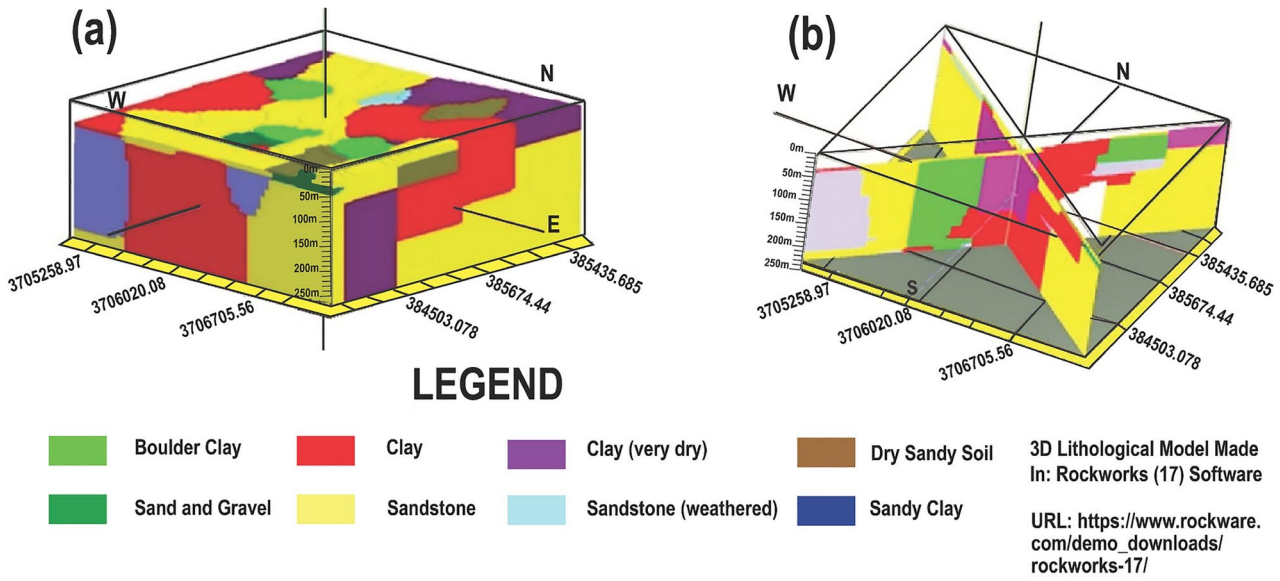

Fig. 10. Interpreted lithological model and lithological fence diagram of study area.

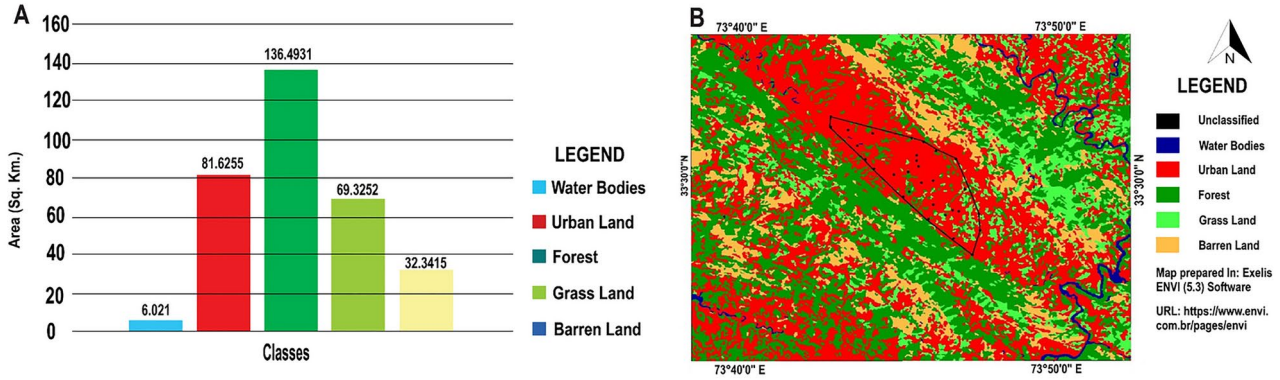

Fig. 11. (**A**). Chart representing classification of land cover map. (**B**) Land-cover map with black polygon showing study area.

southwest directions. Most VES stations were conducted along the drainage patterns to achieve the maximum groundwater yielding rocks in the subsurface. The study area has the dendritic drainage pattern as shown in the Fig. 9 which ultimately leads to the good groundwater potential. The blue lines represent the drainage flow and black arrows represent the flow direction of groundwater based on DEM model. The drainage pattern from northeastern and southwestern sides converges towards the central part of the study area indicating good groundwater potential in the central part of the area.

Discussion

A geophysical and geospatial approach was used to assess the aquifer characteristics and vulnerability in study area. The research aimed to outline the subsurface geology and determine the groundwater potential. Fieldwork consisted of numerous Vertical Electrical Soundings (VES) with a Schlumberger configuration. Local water bodies, surface water, and meteoric water, as well as the nearby Poonch river, recharge the groundwater. Processing and interpreting resistivity data with computer-based software revealed sandstone patches on the southwest and alternating sandstone and clay layers in the south. The aquifers mainly consist of topsoil, clayey sand, sandstone, clays, and boulder clays in various areas with varying thicknesses. Iso-resistivity maps, 2D cross-sections, inversion models, and Dar-Zarrouk parameters were generated from the resistivity data. The VES survey helped in the demarcation of subsurface water bearing layer along with its depth that helped the local engineers for planning boreholes for irrigation and domestic purpose[59]. The VES method helped efficiently to identify the groundwater potential zones and thickness of subsurface layers along with the lithology of the study area[60].

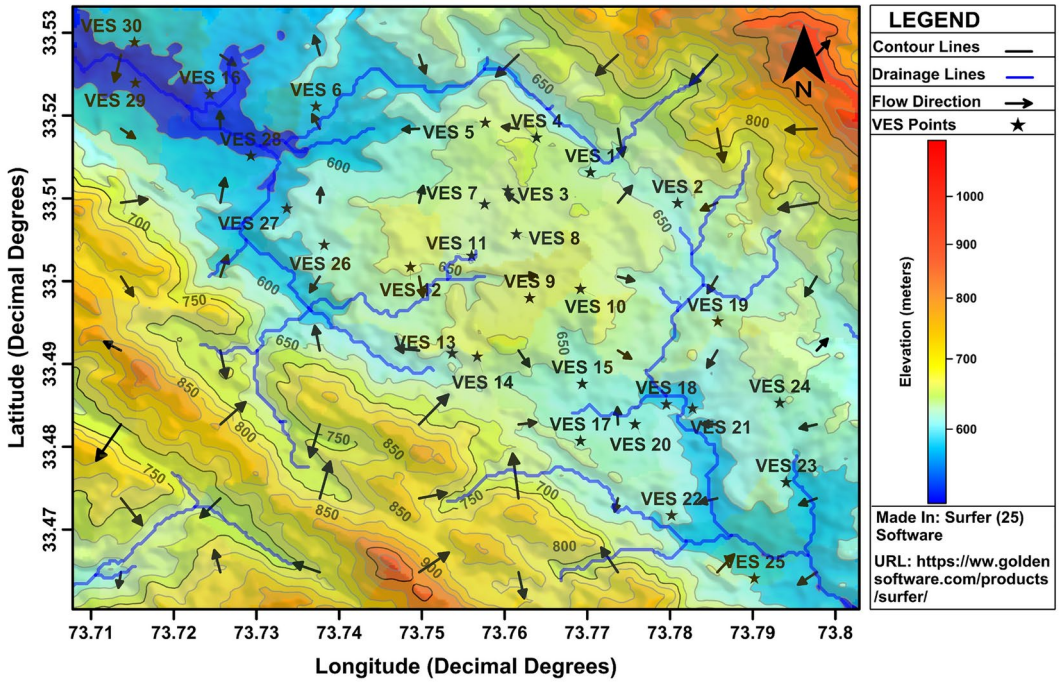

Fig. 12. Drainage and topographic map of study area.

In our case, the geospatial data was processed to generate the land cover map, topographic, flow direction and drainage maps. The presence of dendritic stream patterns indicating towards fair groundwater potential in the study area. The study therefore indicates the presence of alluvium which is an indication of adequate water resource in the study area. Furthermore, the land cover map analysis revealed that green land was found in the northeast and southwest sides of study area indicating the good groundwater recharge. Moreover, the VES stations at central and southern parts of study area are vulnerable for surface contaminants.

The electrical resistivity tomography (ERT) and electromagnetic surveys like audio-magnetotelluric surveys (AMT) techniques are recommended in such hilly terrain to increase the accuracy of results obtained from 1D VES surveys. Numerous tests bore holes for the assessment of groundwater quality should be carried out in the study area. The common geophysical approach in combination with geo-spatial techniques was proved to be efficient method for groundwater exploration with least uncertainties and ambiguities. The current integrated study of geophysical and geospatial approaches provides the excellent water management system, and this integrated approach could be applied in any geographic location across the globe to achieve the results with maximum accuracy.

Conclusions

The integration of vertical electrical sounding and geo-spatial analysis has been successfully implemented to identify the subsurface lithology, groundwater bearing units and aquifer vulnerability in the study area. The VES technique demarcated four to six subsurface geo-electrical layers e.g., topsoil, clay, boulder clay, sandstone, dry sandy soil, mudstone, siltstone, sandy clay, clayey sand, gravel (saturated) and sand and gravel (saturated). The Dar Zarrouk Parameters indicate good groundwater potential at central and north western areas of study area. Similarly, the high values of anisotropy also indicate towards the heterogenous rock formations in the subsurface which lead to the groundwater potential in study area. The aquifers in the area are mainly recharged through surface drainage and thickness values vary among 20–140 m. The drainage network lines and flow directions extracted from digital elevation model also indicate the groundwater potential towards the northern part of study area. The majority of aquifers delineated in the study area are marked as confined due to alternating beds of sandstone and clays. The boreholes are proposed for ground water exploration in the 2nd and 3rd layers in the study area. The protective overburden capacity of the aquifers is rated as poor at VES 1, 3–5, 8, 10–16, 18, 19, 22–25, 27 and 30 whereas the moderate category was found at VES 2, 9 and 20 and excellent at VES 7 and 28, respectively. There is a high probability of the mixing or infiltration of surface contaminants into the aquifers via weak and poorly protective capacity rated VES stations.

Data availability statement

Data sets generated during the current study are available from the corresponding author on reasonable request. The datasets used and/or analysed during the current study available from the corresponding author on reasonable request.

Received: 28 December 2023; Accepted: 11 October 2024

Published online: 26 October 2024

References

1. Jat Baloch, M. Y. et al. Hydrogeochemical mechanism associated with land use land cover indices using geospatial, remote sensing techniques, and health risks model. *Sustainability* **14**(24), 16768 (2022).
2. Baloch, M. Y. J. & Mangi, S. H. Treatment of synthetic greywater by using banana, orange and sapodilla peels as a low cost activated carbon. *J. Mater. Environ. Sci* **10**(10), 966–986 (2019).
3. Jat Baloch, M. Y. et al. Evolution mechanism of arsenic enrichment in groundwater and associated health risks in Southern Punjab, Pakistan. *Int. J. Environ. Res. Public Health* **19**(20), 13325 (2022).
4. Tariq, A., Mumtaz, F., Zeng, X., Baloch, M. Y. J. & Moazzam, M. F. U. Spatio-temporal variation of seasonal heat islands mapping of Pakistan during 2000–2019, using day-time and night-time land surface temperatures MODIS and meteorological stations data. *Remote Sens. Appl.: Soc. Environ.* **27**, 100779 (2022).
5. Iqbal, J. et al. Hydrogeochemical assessment of groundwater and suitability analysis for domestic and agricultural utility in Southern Punjab, Pakistan. *Water* **13**(24), 3589 (2021).
6. Jat Baloch, M. Y. et al. Shallow groundwater quality assessment and its suitability analysis for drinking and irrigation purposes. *Water* **13**(23), 3361 (2021).
7. Talpur, S. A. et al. Hydrogeochemical signatures and suitability assessment of groundwater with elevated fluoride in unconfined aquifers Badin district, Sindh, Pakistan. *SN Appl. Sci.* **2**(6), 1–15 (2020).
8. Masoud, A. A., Koike, K., Atwia, M. G., El-Horiny, M. M. & Gemail, K. S. Mapping soil salinity using spectral mixture analysis of landsat 8 OLI images to identify factors influencing salinization in an arid region. *Int. J. Appl. Earth Observ. Geoinf.* **83**, 101944 (2019).
9. Aoudia, M., Issaadi, A., Bersi, M., Maizi, D. & Saibi, H. Aquifer characterization using vertical electrical soundings and remote sensing: A case study of the chott Ech Chergui basin, northwest Algeria. *J. Afr. Earth Sci.* **170**, 103920 (2020).
10. Szűcs, P., Szabó, N. P., Zubair, M. & Szalai, S. Innovative hydrogeophysical approaches as aids to assess hungarian groundwater bodies. *Appl. Sci.* **11**(5), 2099 (2021).
11. Taufiq, T., Mega, H. D Vertical electrical sounding (VES) resistivity method to analysis freshwater zone at Sriwungu Pamsimas project. In *NSG2021 1st Conference on Hydrogeophysics*, 2021, vol. 2021, no. 1, pp. 1–5: European Association of Geoscientists & Engineers.
12. Braham, M. et al. Identification of groundwater potential zones using remote sensing, GIS, machine learning and electrical resistivity tomography techniques in Guelma basin, northeastern Algeria. *Geocarto Int.* **37**(26), 12042–12072 (2022).
13. Chandra, S. & Tiwari, V. Rapid 3D geophysical imaging of aquifers in diverse hydrogeological settings. *Water Secur.* **15**, 100111 (2022).
14. González, J. A. M., Comte, J.-C., Legchenko, A., Ofterdinger, U. & Healy, D. Quantification of groundwater storage heterogeneity in weathered/fractured basement rock aquifers using electrical resistivity tomography: Sensitivity and uncertainty associated with petrophysical modelling. *J. Hydrol.* **593**, 125637 (2021).
15. de Almeida, A., Maciel, D. F., Sousa, K. F., Nascimento, C. T. C. & Koide, S. Vertical electrical sounding (VES) for estimation of hydraulic parameters in the porous aquifer. *Water* **13**(2), 170 (2021).
16. Savich, V. I., Artikova, H. T., Nafetdinov, S. S., Salimova, K. & Kamdamovich, K. F. Assessment of soil salinity using the vertical electric sounding method. *Eur. J. Agric. Rural Educ.* **2**(5), 12–14 (2021).
17. Omeje, E. T., Ugbor, D. O., Ibuot, J. C. & Obiora, D. N. Assessment of groundwater repositories in Edem, Southeastern Nigeria, using vertical electrical sounding. *Arab. J. Geosci.* **14**(6), 1–10 (2021).
18. Farooq, M. et al. Electrical resistivity tomography for delineating groundwater potential zones in fractured metasedimentary rocks, Lesser Himalayas, Pakistan. *J. Earth Syst. Sci.* **131**(2), 1–14 (2022).
19. Ebong, E. D., Akpan, A. E. & Onwuegbuche, A. A. Estimation of geohydraulic parameters from fractured shales and sandstone aquifers of Abi (Nigeria) using electrical resistivity and hydrogeologic measurements. *J. Afr. Earth Sci.* **96**, 99–109 (2014).
20. Ebong, E. D., Akpan, A. E., Emeka, C. N. & Urang, J. G. Groundwater quality assessment using geoelectrical and geochemical approaches: Case study of Abi area, southeastern Nigeria. *Appl. Water Sci.* **7**, 2463–2478 (2017).
21. Ebong, E. D., George, A. M., Ekwok, S. E., Akpan, A. E. & Asfahani, J. 2D electrical resistivity inversion and ground penetrating radar investigation of near surface cave in New Netim area, southeastern Nigeria. *Acta Geod. et Geophys.* **56**, 765–780 (2021).
22. Díaz-Alcaide, S. & Martínez-Santos, P. Advances in groundwater potential mapping. *Hydrogeol. J.* **27**(7), 2307–2324 (2019).
23. Bersi, M. & Saibi, H. Groundwater potential zones identification using geoelectrical sounding and remote sensing in Wadi Touil plain, Northwestern Algeria. *J. Afr. Earth Sci.* **172**, 104014 (2020).
24. BellucciSessa, E., Castellano, M. & Ricciolino, P. GIS applications in volcano monitoring: The study of seismic swarms at the Campi Flegrei volcanic complex, Italy. *Adv. Geosci.* **52**, 131–144 (2021).
25. Noardo, F. et al. Reference study of CityGML software support: The GeoBIM benchmark 2019—Part II. *Trans. GIS* **25**(2), 842–868 (2021).
26. Hussain, M. A. et al. PS-InSAR based monitoring of land subsidence by groundwater extraction for Lahore metropolitan city, Pakistan. *Remote Sens.* **14**(16), 3950 (2022).
27. Hussain, M. A., Chen, Z., Wang, R. & Shoaib, M. PS-InSAR-based validated landslide susceptibility mapping along Karakorum highway, Pakistan. *Remote Sens.* **13**(20), 4129 (2021).
28. Ahmad, S., Bhatti, S., Shahid, B., Khan, M. Framework for selecting spate irrigation systems and interactive focus group dialogues in Balochistan, Pakistan, ed: Volume.
29. Flanagan, D. C., Frankenberger, J. R., Cochrane, T. A., Renschler, C. S. & Elliot, W. J. Geospatial application of the water erosion prediction project (WEPP) model. *Trans. ASABE* **56**(2), 591–601 (2013).
30. Bahammou, Y. A. et al. Application of vertical electrical sounding resistivity technique to explore groundwater in the Errachidia basin, Morocco. *Groundw. Sustain. Dev.* **15**, 100648 (2021).
31. Ewusi, A., Tetteh, S. E. K., Seidu, J., Ahenkorah I. J. S. A. Hydrogeological risk assessment for mineral exploration in Ghana: A brief overview, p. e02218 (2024).
32. Shahzad, S. M. et al. Appraisal of lacustrine aquifer's groundwater potentiality and its hydrogeological modelling in southeastern Peshawar, Pakistan: Implications for environmental geology, and geotechnical engineering. *Int. J. Geo-Eng.* **15**(1), 12 (2024).
33. Singh, S., Tripura, J. & Shankar, V. Identification of well parameters by the GIS and resistivity (RS) methods in the Hamirpur district (HP). *Sustain. Water Resour. Manag.* **10**(2), 87 (2024).
34. Bayode, S., Mogaji, K. A. & Egbeyemi, O. Modeling of geophysical derived parameters for groundwater potential zonation using GIS-based multi-criteria conceptual model. *Appl. Water Sci.* **14**(2), 19 (2024).
35. Javed, A. et al. Geological and petrographic investigations of the Miocene Molasse deposits in Sub-Himalayas, District Sudhnati, Pakistan. *Arab. J. Geosci.* **14**(15), 1–24 (2021).
36. Iqbal, O., Baig, M. S., Pervez, S. & Siddiqi, M. I. Structure and stratigraphy of Rumbli and Panjar areas of Kashmir and Pakistan with the aid of GIS. *J. Geol. Soc. India* **91**(1), 57–66 (2018).
37. Yasin, M., Ali, S. M. K., Munir, H. & Ishfaque, M. The sedimentary geology, remote sensing, geomorphology and petrology of miocene to late pliocene sediments in District Sudhunhoti and Poonch, Azad Jammu and Kashmir, Pakistan. *Earth Sci. Malaysia* **1**(1), 8–14 (2017).

38. Mughal, M. N., Khan, R., Hussain, A. *Geological Map of the Kotli Area, Parts of Kotli and Sudhnoti Districts, AJK*. Geological Survey of Pakistan (2004).
39. Dad, J. M., Muslim, M., Rashid, I. & Reshi, Z. A. Time series analysis of climate variability and trends in Kashmir Himalaya. *Ecol. Indic.* **126**, 107690 (2021).
40. Muhammad, S., Ullah, N. & Ahmed, A. Spatial distribution of radon concentration and risk evaluation through consumption of groundwater in the District of Kotli, Azad Jammu and Kashmir. *Kuwait J. Sci.* **51**(1), 100152 (2024).
41. Baig, J. A. et al. Evaluation of arsenic and other physico-chemical parameters of surface and ground water of Jamshoro, Pakistan. *J. Hazard. Mater.* **166**(2–3), 662–669 (2009).
42. Telford, W. M., Geldart, L. P. & Sheriff, R. E. *Applied geophysics* (Cambridge University Press, 1990).
43. Bernstone, C., Dahlin, T., Ohlsson, T. & Hogland, H. DC-resistivity mapping of internal landfill structures: Two pre-excavation surveys. *Environ. Geol.* **39**(3), 360–371 (2000).
44. Omosuyi, G., Adeyemo, A. & Adegoke, A. Investigation of groundwater prospect using electromagnetic and geoelectric sounding at afunbiowo, near Akure, Southwestern Nigeria. *Pac. J. Sci. Technol.* **8**(2), 172–182 (2007).
45. Khan, S. et al. Aquifer vulnerability and groundwater quality around Brahma Bahtar Lesser Himalayas Pakistan. *Environ. Earth Sci.* **80**(13), 1–13 (2021).
46. Nisar, U. B. et al. Quaternary paleo-depositional environments in relation to ground water occurrence in lesser Himalayan Region, Pakistan. *J. Himal. Earth Sci.* **51**(1), 1 (2018).
47. Niaz, A., Khan, M. R., Mustafa, S. & Hameed, F. Determination of aquifer properties and vulnerability mapping by using geoelectrical investigation of parts of Sub-Himalayas, Bhimber, Azad Jammu and Kashmir, Pakistan. *Quart. J. Eng. Geol. Hydrogeol.* **49**(1), 36–46 (2016).
48. Straub, C. L., Koontz, S. R., Loomis, J. B. Economic valuation of landsat imagery. In: Open-file report, Reston, VA, Report 2019-1112, 2019, Available: https://pubs.usgs.gov/publication/ofr20191112.
49. Chukwuma, E. et al. Geo-electric groundwater vulnerability assessment of overburden aquifers at Awka in Anambra State, south-eastern Nigeria. *Eur. J. Biotechnol. Biosci.* **3**(1), 29–34 (2015).
50. Niaz, A., Imtiaz, M., Khan, M. R., Hameed, F., Niaz, J., Khan, A. Y., & Mehmood, K. The use of GIS and geo-electric techniques for modeling of surface and groundwater in Kotli City, District Kotli, Azad Jammu and Kashmir, Pakistan. *Pakistan J. Eng. Appl. Sci.* (2020).
51. Akinlalu, A., Mogaji, K. & Adebodun, T. Assessment of aquifer vulnerability using a developed "GODL" method (modified GOD model) in a schist belt environ, Southwestern Nigeria. *Environ. Monit. Assess.* **193**(4), 1–27 (2021).
52. Slater, L. Near surface electrical characterization of hydraulic conductivity: From petrophysical properties to aquifer geometries—a review. *Surveys Geophys.* **28**(2), 169–197 (2007).
53. Nisar, U. B. et al. Groundwater investigations in the Hattar industrial estate and its vicinity, Haripur district, Pakistan: An integrated approach. *Kuwait J. Sci.* **48**(1), 1 (2021).
54. Arulprakasam, R., Siva, K. & Gowtham, B. Electrical resistivity technique for demarcation of groundwater quality zones in parts of Vanur block, Villupuram district, Tamil Nadu. *Int. J. Geol. Agric. Environ. Sci.* **2**(1), 28–30 (2014).
55. SrinivasaGowd, S. Electrical resistivity surveys to delineate groundwater potential aquifers in Peddavanka watershed, Anantapur District, Andhra Pradesh, India. *Environ. Geol.* **46**(1), 118–131 (2004).
56. Hussain, Y., Ullah, S. F., Akhter, G. & Aslam, A. Q. Groundwater quality evaluation by electrical resistivity method for optimized tubewell site selection in an ago-stressed Thal Doab Aquifer in Pakistan. *Model. Earth Syst. Environ.* **3**(1), 1–9 (2017).
57. Nwankwo, C., Nwosu, L. & Emujakporue, G. Determination of Dar Zarouk parameters for the assessment of groundwater resources potential: Case study of Imo State, south eastern Nigeria. *J. Econ. Sustain. Dev.* **2**(8), 1 (2011).
58. Adadzi, P., Coffie, H., Afetorgbor, E., Takase, M. Vertical electrical sounding survey for groundwater exploration for rural water supply in parts of Ketu south in the Volta region of Ghana (2018).
59. Phanjaya, H., Parnadi, W. W., Santoso, D. Electrical resistivity survey for groundwater investigation in Padalarang, West Java. In: *IOP Conference Series: Earth and Environmental Science*, 2022, vol. 1031, no. 1, p. 012006: IOP Publishing.
60. Prayogo, T., Bisri, M., Fadhia, K., Martius, A. Aquifer potential investigation applying vertical electrical sounding in Bango sub-catchment area. In: *IOP Conference Series: Earth and Environmental Science*, 2024, vol. 1311, no. 1, p. 012038: IOP Publishing.
61. Braga, A. C. D. O. & Francisco, R. F. Natural vulnerability assessment to contamination of unconfined aquifers by longitudinal conductance–(s) method. *J. Geogr. Geol.* **6**(4), 68–79 (2014).
62. Omeiza, J. A. & Dary, D. M. Aquifer vulnerability to surface contamination: a case of the new millennium city, Kaduna, Kaduna State Nigeria. *World J. Appl. Phys.* **3**(1), 1–12 (2018).

Author contributions

Conceptualization, Ali Yousaf Khan and Abrar Niaz; Methodology, Ali Yousaf Khan and Abrar Niaz; software, Waheed Ullah., Rashida Fiaz., Ali Yousaf Khan; Validation, Tehmina Bibi and Shehla Gul, Muhammad Mubashar Imtiaz; Formal analysis, Ali Yousaf Khan and Abrar Niaz; investigation; Ali Yousaf Khan., Kiran Hameed and Fakhrul Islam; resources, Kiran Hameed and Ali Yousaf Khan; data curation Ali Yousaf Khan, Muhammad Mubashar Imtiaz; writing, review, Tehmina Bibi , Ali Yousaf Khan and Waheed Ullah ; visualization, Ali Yousaf khan, Shehla Gul and Tehmina Bibi, supervision; Abrar Niaz., Rashida Fiaz and Tehmina Bibi.

Declarations

Competing interests

The authors declare no competing interests.

Consent to publish

The Authors has consented to the submission to the journal.

Additional information

Correspondence and requests for materials should be addressed to W.U.

Reprints and permissions information is available at www.nature.com/reprints.

Publisher's note Springer Nature remains neutral with regard to jurisdictional claims in published maps and institutional affiliations.